Lab on a Chip

Accepted Manuscript

ROYAL SOCIETY OF CHEMISTRY

www.rsc.org/loc

Lab on a Chip

RSCPublishing

ARTICLE

Microfluidic Continuous Flow Digital Loop-Mediated Isothermal Amplification (LAMP)

Cite this: DOI: 10.1039/xoxxoooooox

Tushar D. Rane[a], Liben Chen[b], Helena C. Zec[a], Tza-Huei Wang[a,b]*

Received ooth January 2012,
Accepted ooth January 2012

DOI: 10.1039/xoxxoooooox

www.rsc.org/

Digital nucleic acid detection is rapidly becoming a popular technique for ultra-sensitive and quantitative detection of nucleic acid molecules in a wide range of biomedical studies. Digital polymerase chain reaction (PCR) remains the most popular way of conducting digital nucleic acid detection. However, due to the need for thermocycling, digital PCR is difficult to implement in a streamlined manner on a single microfluidic device, leading to complex fragmented workflows and multiple separate devices and instruments. Loop-mediated isothermal amplification (LAMP) is an excellent isothermal alternative to PCR with potentially better specificity than PCR through the use of multiple primer sets for a nucleic acid target. Here we report a microfluidic droplet device implementing all the steps required for digital nucleic acid detection including droplet generation, incubation and in-line detection for digital LAMP. As compared to microchamber or droplet array-based digital assays, continuous flow operation of this device eliminates the constraints on the number of total reactions by the footprint of the device and the analysis throughput by the time for lengthy incubation and transfers of materials between instruments.

Introduction

Digital polymerase chain reaction (PCR) is rapidly becoming the technique of choice for ultra-sensitive quantification of rare nucleic acid molecules present in biological samples [1-5]. Digital PCR involves breaking down a sample mixed with PCR reagents into a large number of discrete reactions where single molecules are stochastically confined. As PCR is run in parallel on all these reactions through thermocycling, accurate quantification of the nucleic acid molecule of interest can be obtained through simple statistical analysis based on the number of positive PCR reactions from the total pool of reactions.

Since the initial demonstrations of this concept in tube [6] and capillary format [7], a variety of microfluidic platforms have been proposed for practical implementation of the digital PCR technique. These platforms can be broadly classified into two different types. The first type involves microfabrication of a large array of micro-wells on a substrate [8-10]. This format is capable of real-time digital PCR monitoring. More recently this platform has also been implemented for digital isothermal amplification[11, 12]. However, the sample volume that can be analyzed and the well size are fixed by the microfluidic design. Any change in sample volume or individual reaction volume (well size) requires a change in design.

The second type involves generation of a large number of tiny emulsion droplets (nanoliter to picoliter-sized) from the sample mixed with PCR reagents[1, 2]. Each of the individual droplets then functions as an independent reaction chamber. While the microfluidic droplet platform offers the flexibility in changing the reaction volume without modifying the chip design, previously developed systems either have poor amplification efficiency[13] or require a complicated workflow[14]. Commercial instruments available for conducting this type of analysis, such as ddPCR™ from Bio-Rad, involve fragmented workflow requiring separate instruments/devices for completion of analysis viz. 1) A droplet generation device 2) A thermocycler and 3) A droplet reader device to detect reaction outcome from droplets. This mode of operation is inefficient for high throughput analysis due to the need of material transfers between devices and the time wasted on idle instruments.

Implementing the droplet-based digital nucleic acid analysis workflow on a single device addresses the issues mentioned above. Such a device can be capable of performing all three steps of analysis viz. droplet generation; droplet incubation as well as droplet detection in a continuous flow manner. Continuous flow operation implies that there is no idle time involved in the sample processing workflow. Since the entire process is performed in an assembly-line manner, the throughput of analysis is not limited by the thermal cycling or incubation time that typically is the time-limiting step in nucleic acid amplification. When coupled to the techniques of arrayed sample delivery using a capillary cartridge [15-20], the continuous flow design promises high throughput digital analyses of multiple samples on a single device. Furthermore, since the number of droplets that can be analyzed is no longer limited by the footprint of the incubation zone on the microfluidic chip, continuous flow digital assays allow for, in principle, unlimited sample volume and number of reactions and thus wide dynamic range of quantification.

Despite this potential for improved throughput, larger sample volume processing capability and wider dynamic range, implementing continuous flow digital assays in droplet format is difficult due to issues caused by thermocycling on a chip, such as

evaporation and droplet collision and fusion. Very few attempts have been made in the past to realize digital PCR in a continuous flow format. These few attempts have had limited success in terms of target nucleic acid quantification [13, 21].

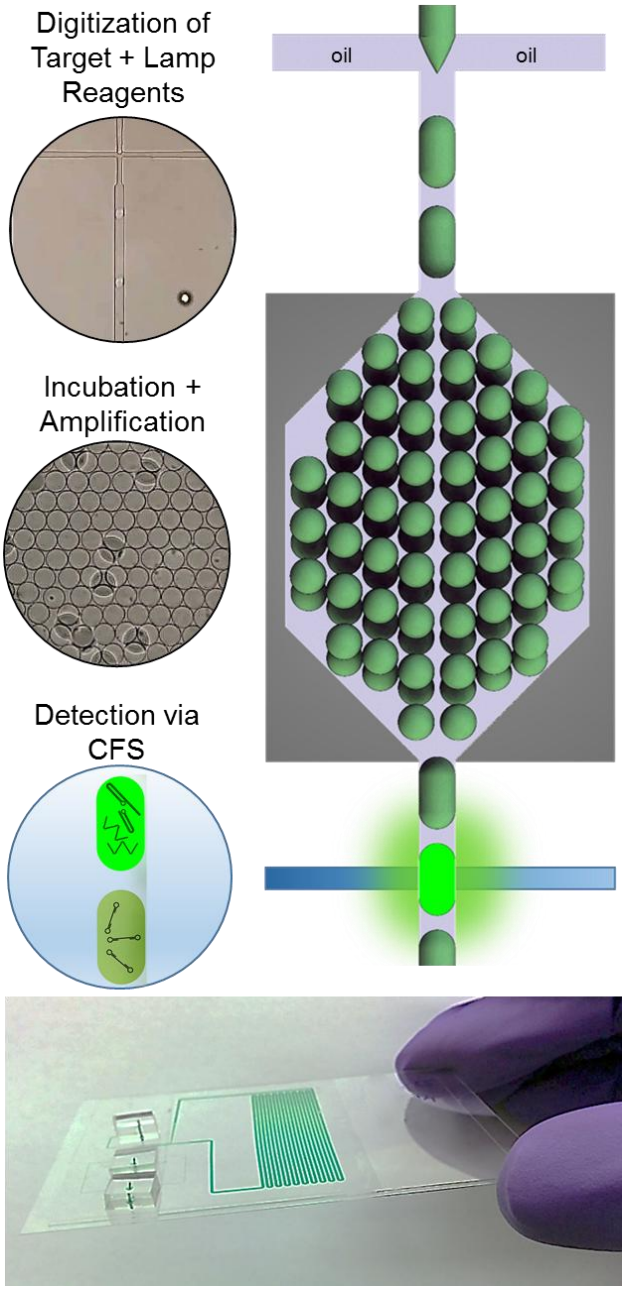

Figure 1. Droplet microfluidic device for continuous flow digital LAMP analysis: A schematic illustrating three steps of digital LAMP analysis that are conducted on the droplet microfluidic device is shown at top right. Images of the droplet generation and incubation region an actual microfluidic device are shown in the top two circles on the left hand side. An image of an actual thin microfluidic device is shown at the bottom.

Loop-mediated isothermal amplification (LAMP) is an excellent alternative to PCR for nucleic acid amplification[22-25]. LAMP functions through auto-cycling strand displacement DNA synthesis. In a LAMP reaction, a DNA polymerase with a high strand displacement activity is used with a set of two inner and outer primers. All four primers are used during the initial stages of the reaction while only inner primers are used during the later stages of the reaction. The reaction results in production of stem-loop DNAs with multiple inverted target repeats. LAMP, through its simple requirement for single temperature incubation, is very suitable for implementation in a continuous flow format. Furthermore, since LAMP uses a set of 4 different primers recognizing six independent sequences on a target nucleic acid, it can also provide better specificity than PCR [22, 23].

In this report, we demonstrate the first continuous flow digital LAMP assay implemented on a microfluidic droplet device. The schematic shown in Figure 1 illustrates the simple functioning scheme of the device. A sample to be analyzed is mixed with LAMP reagents and then digitized into picoliter-sized droplets on the device. The image shown in Figure 1 as well as Supporting Video 1 show the droplet generation process on the device. The droplets then flow to an incubation region where they are exposed to temperature suitable for the LAMP reaction. The image shown in Figure 1 and Supporting Video 2 show droplets in this region of the device. The incubation region is a wide serpentine channel designed to allow multiple droplets to flow side-by-side, thus maintaining low flow resistance, but at the same time sufficiently narrow to allow droplets to flow in a sequence from droplet generation to detection region. Finally these droplets move to a downstream detection region on the device, where fluorescence detection is conducted on these droplets using confocal fluorescence spectroscopy. All three steps required for analysis occur simultaneously on the device. This implies that the throughput of the device is only limited by the rates of droplet generation and fluorescence detection.

Experimental section

A. Device Fabrication

An image of the whole microfluidic device is included in Figure 1. The devices were fabricated using polydimethylsiloxane (PDMS) as the structural material. To avoid evaporation of droplets during transit through the incubation region, we devised a fabrication scheme to fabricate thin PDMS devices. Initially the molds for the devices were fabricated on 4" Si wafers using standard photolithography technique with SU8-3025 (MicroChem Corp.) as the structural material. Initially a relatively thick layer of PDMS [Sylgard 184(Ellsworth Adhesives), 10:1 base to curing agent ratio] is coated on a blank wafer at a slow spin speed of 100 rpm on a spin coater (Laurell Technologies, Corp). This layer is cured at 80^{o}C for 10 min. While the thick PDMS layer is being cured, a thin layer of PDMS (6:1 base to curing agent ratio) is spin coated on the device mold at 350rpm. This thin layer of PDMS is cured at 80^{o}C for 6 min. A rectangular piece, large enough to cover the whole device area, is then cut out from the cured thick PDMS layer. This rectangular piece is partially bonded to the cured thin PDMS layer on the device mold by baking at 80^{o}C for 5 min. Finally the bonded thick and thin layers are peeled off the mold. The thick layer just acts as a support to allow for manipulation of the thin layer. Access holes are then punched on the device at the input and output ports. The thin layer is then bonded to thickness #1 cover glass (Ted Pella, Inc) using standard O2 plasma treatment. The thick layer being partially bonded to the thin layer, can then be easily peeled off without breaking the bond between the thin layer and the cover glass. Small cubes of PDMS (10:1 base to curing agent ratio) with holes punched at the center are then bonded to the thin PDMS layer using O2 plasma treatment. Finally another thickness #1 coverglass is bonded to the thin PDMS layer, effectively sandwiching this layer between two pieces of coverglass in the incubation region on the device. A schematic of the fabrication sequence is included in Supporting Figure S1.

B. Materials

The following reagents were used for LAMP reactions on and off-chip: Betaine (Sigma-Aldrich Co., LLC), MgSO4 (New England Biolabs), ROX reference dye (Life Technologies), dNTPs (Life Technologies), BSA (New England Biolabs), Calcein (Anaspec, Inc), Manganese Chloride (Sigma-Aldrich Co., LLC), EvaGreen dye (Biotium Inc), Bst 2.0 WarmStart DNA Polymerase and isothermal reaction buffer (New England Biolabs). A typical reaction mixture consisted of 1X isothermal reaction buffer, 0.8M Betaine, 7mM MgSO4 , 25µM Calcein, 0.75mM Manganese Chloride, 0.25µM ROX reference dye, 0.1mg/mL BSA, 1.4mM dNTPs and 0.32 U/µL BST WarmStart DNA Polymerase. For experiments with EvaGreen, Calcein and Manganese chloride were replaced with 0.5X EvaGreen dye where 1X is the manufacturer recommended concentration.

The primers for the experiments were designed to be specific to a region on the 16s rRNA gene for Neisseria Gonorrhoeae. The genome sequence of Neisseria Gonorrhoeae (strain FA1090) was obtained from the NIH genetic sequence database Genbank®. The primers were designed using the LAMP primer design software PrimerExplorer. For the experiments with synthetic target, a double stranded target was generated using fusion PCR and then purified from the gel band specific to the target after running electrophoresis on the PCR product. For the experiments with genomic DNA, DNA extracted from Neisseria Gonorrhoeae (Strain FA1090, ATCC® 700825™) was purchased from ATCC®. The base sequences of primers used for LAMP experiments are as follows

F3: 5- ATC CTG GCT CAG ATT GAA CG -3
B3: 5- ATA TCG GCC GCT CGG ATA -3
FIP: 5- GCC ACC CGA GAA GCA AGC TTC TTT TGG CGG CAT GCT TTA CAC AT -3
BIP: 5- TAC CGG GTA GCG GGG GAT AAT TTT CTG CTT TCC CTC TCA AGA CG -3
LoopF: 5- TGC TGC CGT CCG ACT TG -3
LoopB: 5- CTG ATC GAA AGA TCA GCT AAT ACC G -3

The base sequence of the target region flanked by the primers F3 and B3 is

5- ATC CTG GCT CAG ATT GAA CGC TGG CGG CAT GCT TTA CAC ATG CAA GTC GGA CGG CAG CAC AGG GAA GCT TGC TTC TCG GGT GGC GAG TGG CGA ACG GGT GAG TAA CAT ATC GGA ACG TAC CGG GTA GCG GGG GAT AAC TGA TCG AAA GAT CAG CTA ATA CCG CAT ACG TCT TGA GAG GGA AAG CAG GGG ACC TTC GGG CCT TGC GCT ATC CGA GCG GCC GAT AT -3

For all experiments, the final concentration of all primers in the reaction mixture was kept constant at 1) 0.2µM for F3, B3 2) 1.6uM for FIP and BIP and 3) 0.8uM for LoopF and LoopB respectively. The oil phase used for experiments on-chip consisted of FC40 (3M) with 5% perfluoropolyether-polyethyleneglycol surfactant (RAN Biotechnologies, Inc) by weight.

C. Device operation

Reagents (oil phase and sample) were delivered to the device through custom assembled flow controllers with flow feedback (IDEX Health and Science, LLC). For the duration of an experiment, the device was mounted on a platform designed such that the incubation region on the device was placed on a custom peltier heater assembly. This peltier heater assembly was used to maintain the incubation region on the device at a temperature of 63°C suitable for the LAMP reaction. Fluorescence was continuously detected from droplets passing through the detection region on the device by a custom built confocal fluorescence spectroscopy setup. The optical setup is capable of dual excitation (488nm and 552nm) as well as dual band detection (506-534nm and 608-648nm). A schematic of the optical setup is included in Supporting Figure S2.

Results and discussion

Reliable quantification with digital LAMP reaction requires assay readout with good signal to background ratio (SBR). We compared two different assay outcome indicators for the LAMP assay viz. 1) DNA binding dye EvaGreen® and 2) A Calcein dye based indicator [23]. The details of the experiments are included in Supporting Section 1. Briefly, EvaGreen indicates a positive LAMP reaction through increased fluorescence resulting from the binding of the dye to the large amount of double stranded DNA generated by the LAMP reaction. On the other hand Calcein dye is non-fluorescent when bound with Manganese ions. However, large amount of DNA generated during LAMP reaction results in generation of pyrophosphate as a byproduct, which sequesters Manganese from Calcein, resulting in return of the dye to its original fluorescence.

We tested both readouts for SBR under different conditions using the synthetic dsDNA target containing a base sequence specific to Neisseria Gonorrhoeae (Supporting Figures S3, S4, S5 and S6). Our results indicate that the maximum SBR possible with EvaGreen was approx. 2 whereas the maximum SBR possible with Calcein was approx. 6.5.

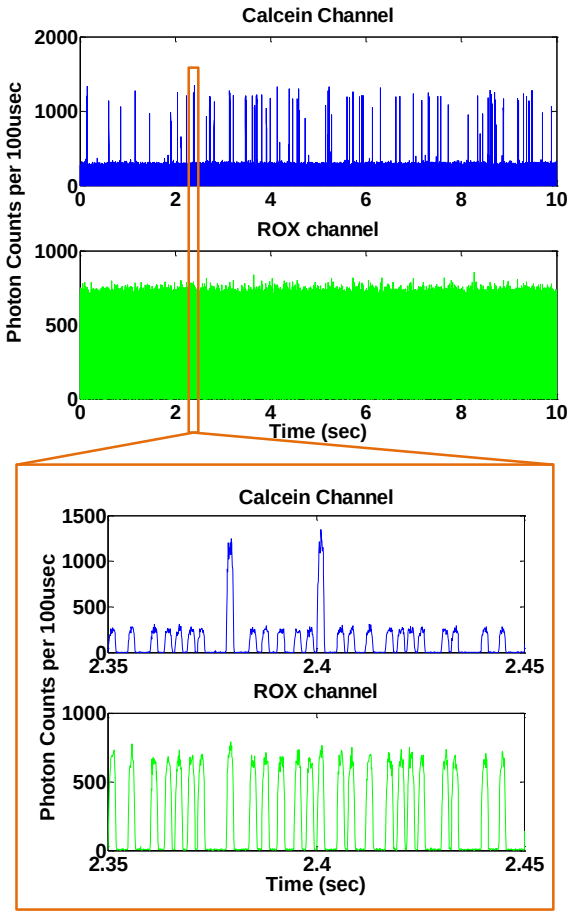

Figure 2. Sample digital LAMP signal from droplets with a Calcein based readout. Blue trace: Calcein fluorescence signal, Green trace: ROX (indicator dye) fluorescence signal. The inset shows individual droplets in the fluorescence data traces. The indicator dye fluorescence intensity can be seen uniform across droplets whereas the Calcein fluorescence intensity varies between two levels: high intensity indicating positive LAMP reaction and low intensity indicating negative LAMP reaction.

We then fabricated a microfluidic device to conduct droplet experiments as described in the Experimental section. To ensure uniform processing of droplets, the incubation region of the device

was designed to have channel height only sufficient for 1-2 layers of droplets. Although this approach can minimize the variation in droplet heating due to differences in distance from the heater for different layers of droplets, it also makes the droplets more susceptible to evaporation, due to increased contact with the surface. So to avoid any possible evaporation of droplets, we modified standard soft lithography technique to fabricate very thin microfluidic devices (Figure 1). The thin incubation region of the device was further sandwiched between two pieces of cover glass. The reduction in thickness of porous PDMS in the incubation region as well as the physical barrier of cover glass can effectively reduce evaporation during transit of droplets through this region.

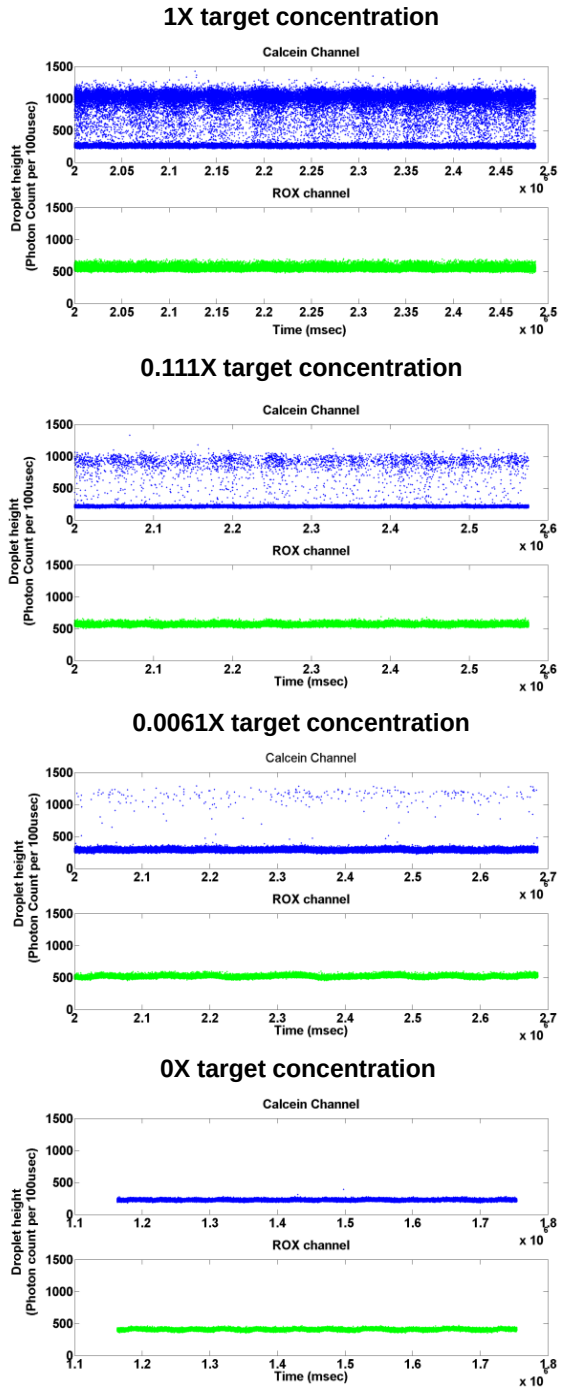

Figure 3. Average droplet fluorescence intensity data from large droplet populations for different target concentrations. Each droplet has two data points associated with it. A blue data point indicating average Calcein fluorescence intensity and a corresponding green data point indicating average ROX intensity. Data from a population of 100000 droplets is shown for each target concentration. The ROX intensity shows minimal variability across droplets whereas the Calcein intensity varies between two levels as expected from Figure 2. The fraction of the positive droplet population can be seen decreasing with decreasing target concentration.

Furthermore, effective functioning of this approach required integration of an optical detection system, a temperature control system, a pumping system as well as the microfluidic device. We integrated all these systems as described in the Experimental section. A schematic of the optical system can also be seen in Supporting Figure S2. One of the challenges with proper functioning of this system was large drift of optical focus of the optical detection system during long term data acquisition from a device due to temperature changes of the device holder stage, caused by heat accumulated from the peltier heater used for heating the device. Conventional fan-based cooling systems were ill-suited to this application due to the vibrations induced by a cooling fan. Hence a water cooling system, similar to that used for cooling of central processing units (CPUs) in high-end computers was used. This approach allowed us to collect fluorescence data from the device for long periods of time, without significant drift in optical focus.

We then tested both of these assay outcome indicators on the droplet device shown in Figure 1. To conduct this test, a low concentration of the synthetic target was mixed with LAMP reagents and then processed on the droplet device. An indicator dye (ROX) is encapsulated in the droplets in these experiments to visualize droplet boundary in a fluorescence data trace. Supporting Figure S7 shows sample digital fluorescence signal obtained from Evagreen-based assay readout. In this case, the fluorescence channel corresponding to the indicator dye shows steady fluorescence intensity across droplets whereas assay readout specific fluorescence channel shows characteristic digital signal with droplet intensities varying between two different levels. Similarly, Figure 2 shows a sample digital fluorescence data trace obtained from Calcein-based assay readout. Calcein-based detection clearly shows much stronger difference between positive droplets (positive LAMP reaction) and negative droplets (negative LAMP reaction). As data is collected from a large number of droplets, the two droplet populations (positive and negative) can be easily distinguished from each other in both cases as long as the positive droplet population is a significant fraction of the total droplet population. However, for droplet populations with rare positive droplets, it was not possible to reliably threshold the droplet intensity data to identify positive droplets from the droplet population with EvaGreen based readout due to low SBR. So for all subsequent experiments we used Calcein-based readout to detect the outcome of the LAMP reaction.

We then tested the capability of the continuous flow device to function for long periods of time while processing samples with different target concentrations. Figure 3 shows average droplet fluorescence intensity data for different target concentrations. The data corresponding to each target concentration is obtained from a population of 100000 droplets each. Each droplet has two data points associated with it 1) A Blue data point indicating average Calcein fluorescence intensity and 2) A Green data point indicating average ROX fluorescence intensity. As expected for all different target concentrations, the ROX fluorescence intensity shows minimal variation whereas the Calcein fluorescence intensity shows two distinct populations.

Target quantification from the droplet intensity data requires proper separation of the two populations of droplets (positive and negative) from each other. We tested two different techniques to

conduct this separation 1) Standard thresholding with a fixed threshold and 2) Automated clustering using expectation maximization algorithm in Matlab. For thresholding analysis, a threshold approximately centered between the two peaks in the droplet intensity histograms was used whereas for automated clustering, two Gaussians were fit to the histogram data using default fitting conditions in Matlab (Supporting Figure S8; details in Supporting Section 2). The positive droplet fraction identified for different input target concentrations using these two techniques is plotted against the expected target concentration in Supporting Figure S9. The data points follow a characteristic exponential curve predicted by the Poisson distribution of target molecules within droplets. We observed that the two techniques for positive droplet identification agree fairly well with each other for higher target concentrations. However, for lower target concentrations, the automated clustering technique results in large overestimation of positive droplets as a number of negative droplets are misclassified as positive droplets by the clustering algorithm.

We then tested our device for quantification of genomic DNA extracted from Neisseria Gonorrhoeae (Strain FA1090, ATCC® 700825™). All the experimental conditions were maintained same as those for the synthetic target, except that the synthetic target was replaced with genomic DNA. Similar to the synthetic target related experiments, we experimentally obtained a positive droplet fraction for various genomic DNA concentrations tested on the device and then plotted them against the estimated target DNA concentration (Figure 4). The lowest target concentration detected in our experiments was ~600 copies/µL. The limit of detection is affected by multiple factors. One of the factors is presence of a fraction of droplets with incomplete amplification as seen in Figure 3. These droplets appear between the two dense bands of 'positive' and 'negative' droplets. The intermediate intensity of these droplets results in misclassification of a fraction of these droplets as negative droplets after thresholding, resulting in a higher limit of detection. Furthermore, isolated droplets with positive amplification in the negative control (on the order of 1-10 droplets per million) also put a constraint on the limit of detection. This issue is likely due to false-positive non-specific amplification. These issues can be potentially addressed through optimization of the LAMP reaction conditions on the device, which may reduce false positives and bring LAMP reaction to completion in most of the positive droplets.

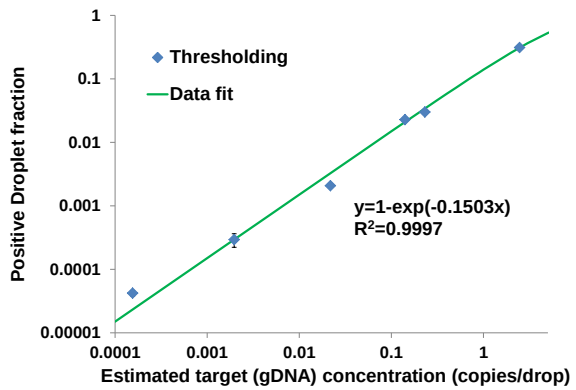

Figure 4. Neisseria Gonorrhoeae genomic DNA (gDNA) quantification with digital LAMP. The plot of the positive droplet fraction against the expected gDNA concentration in copies per droplet also shows an exponential relationship predicted by Poisson distribution.

Conclusion

In summary, we demonstrated a continuous flow digital nucleic acid detection system using LAMP reaction as a means of nucleic acid amplification. Using this system, we obtained throughputs on the order of one million droplets per 110 minutes. With an average drop volume of 10pL, this corresponds to processing of 10uL of sample volume per 110 mins. In the current setting, the throughput of this system is only limited by the speed at which fluorescence can be detected from droplets reliably. Since we are operating in a conservative region where the transit time per droplet is ~1-2 msec per droplet, there is plenty of room to further enhance the throughput, making this an attractive alternative to the traditional digital PCR workflow for digital nucleic acid sensing. The continuous flow digital LAMP can be further interfaced with a capillary that is pre-loaded with an array of samples plugs isolated by oil [15] to allow for seamless processing of multiple samples on a single device. On the other hand, applications which require rare molecule sensing, e.g. detection of circulating mutated DNA in a high excess of normal DNA in blood samples [26], can benefit from the capability of this device to screen as large the total number of reactions as required due to continuous flow format of operation.

Acknowledgments

We would like to thank Dr. Darren Lewis and IDEX Health & Science LLC for providing us with the custom built flow controllers used for our experiments. We would also like to thank Dr. Charlotte A. Gaydos and Justin Hardick for providing us with Neisseria Gonorrhoeae gDNA. Finally we would like to thank our funding agencies NIH (R01CA155305 and U54 EB 007958) and NSF (1159771).

Supporting Information

Electronic Supplementary Information (ESI) in the form of videos and figures as described in text available. See DOI: 10.1039/b000000x/

Author information

[a] Department of Biomedical Engineering
[b] Department of Mechanical Engineering, Johns Hopkins University, Baltimore, MD 21218
* Corresponding Author (thwang@jhu.edu)

References

1 B. J. Hindson, K. D. Ness, D. A. Masquelier, P. Belgrader, N. J. Heredia, A. J. Makarewicz, I. J. Bright, M. Y. Lucero, A. L. Hiddessen, T. C. Legler, T. K. Kitano, M. R. Hodel, J. F. Petersen, P. W. Wyatt, E. R. Steenblock, P. H. Shah, L. J. Bousse, C. B. Troup, J. C. Mellen, D. K. Wittmann, N. G. Erndt, T. H. Cauley, R. T. Koehler, A. P. So, S. Dube, K. A. Rose, L. Montesclaros, S. Wang, D. P. Stumbo, S. P. Hodges, S. Romine, F. P. Milanovich, H. E. White, J. F. Regan, G. A. Karlin-Neumann, C. M. Hindson, S. Saxonov and B. W. Colston, *Anal. Chem.*, 2011, **83**, 8604-8610 (DOI:10.1021/ac202028g).
2 Q. Zhong, S. Bhattacharya, S. Kotsopoulos, J. Olson, V. Taly, A. D. Griffiths, D. R. Link and J. W. Larson, *Lab. Chip*, 2011, **11**, 2167-2174 (DOI:10.1039/c1lc20126c).
3 M. Baker, *Nat Meth*, 2012, **9**, 541-544.
4 M. C. Strain, S. M. Lada, T. Luong, S. E. Rought, S. Gianella, V. H. Terry, C. A. Spina, C. H. Woelk and D. D. Richman, *PLoS One*, 2013, **8**, e55943 (DOI:10.1371/journal.pone.0055943 [doi]).
5 N. J. Heredia, P. Belgrader, S. Wang, R. Koehler, J. Regan, A. M. Cosman, S. Saxonov, B. Hindson, S. C. Tanner, A. S. Brown and G. Karlin-Neumann, *Methods*, 2013, **59**, S20-3 (DOI:10.1016/j.ymeth.2012.09.012 [doi]).
6 P. J. Sykes, S. H. Neoh, M. J. Brisco, E. Hughes, J. Condon and A. A. Morley, *BioTechniques*, 1992, **13**, 444-449.
7 O. Kalinina, I. Lebedeva, J. Brown and J. Silver, *Nucleic Acids Res.*, 1997, **25**, 1999-2004 (DOI:gka325 [pii]).
8 E. A. Ottesen, J. W. Hong, S. R. Quake and J. R. Leadbetter, *Science*, 2006, **314**, 1464-1467 (DOI:10.1126/science.1131370).

9 K. A. Heyries, C. Tropini, M. Vaninsberghe, C. Doolin, O. I. Petriv, A. Singhal, K. Leung, C. B. Hughesman and C. L. Hansen, *Nat. Methods*, 2011, **8**, 649-651 (DOI:10.1038/nmeth.1640 [doi]).
10 F. Shen, W. Du, J. E. Kreutz, A. Fok and R. F. Ismagilov, *Lab. Chip*, 2010, **10**, 2666-2672 (DOI:10.1039/c004521g [doi]).
11 A. Gansen, A. M. Herrick, I. K. Dimov, L. P. Lee and D. T. Chiu, *Lab. Chip*, 2012, **12**, 2247-2254 (DOI:10.1039/c2lc21247a; 10.1039/c2lc21247a).
12 Q. Zhu, Y. Gao, B. Yu, H. Ren, L. Qiu, S. Han, W. Jin, Q. Jin and Y. Mu, *Lab. Chip*, 2012, **12**, 4755-4763 (DOI:10.1039/c2lc40774d [doi]).
13 M. M. Kiss, L. Ortoleva-Donnelly, N. R. Beer, J. Warner, C. G. Bailey, B. W. Colston, J. M. Rothberg, D. R. Link and J. H. Leamon, *Anal. Chem.*, 2008, **80**, 8975-8981.
14 P. Kumaresan, C. J. Yang, S. A. Cronier, R. G. Blazej and R. A. Mathies, *Anal. Chem.*, 2008, **80**, 3522-3529 (DOI:10.1021/ac800327d).
15 H. Zec, T. D. Rane and T. Wang, *Lab on a Chip*, 2012, **12**, 3055-3062.
16 J. Q. Boedicker, L. Li, T. R. Kline and R. F. Ismagilov, *Lab. Chip*, 2008, **8**, 1265-1272 (DOI:10.1039/b804911d).
17 T. R. Kline, M. K. Runyon, M. Pothiawala and R. F. Ismagilov, *Anal. Chem.*, 2008, **80**, 6190-6197 (DOI:10.1021/ac800485q).
18 L. Li, D. Mustafi, Q. Fu, V. Tereshko, D. L. Chen, J. D. Tice and R. F. Ismagilov, *Proc. Natl. Acad. Sci. U. S. A.*, 2006, **103**, 19243-19248 (DOI:10.1073/pnas.0607502103).
19 D. L. Chen and R. F. Ismagilov, *Curr. Opin. Chem. Biol.*, 2006, **10**, 226-231 (DOI:10.1016/j.cbpa.2006.04.004).
20 V. Linder, S. K. Sia and G. M. Whitesides, *Anal. Chem.*, 2005, **77**, 64-71 (DOI:10.1021/ac049071x).
21 Y. Schaerli, R. C. Wootton, T. Robinson, V. Stein, C. Dunsby, M. A. Neil, P. M. French, A. J. Demello, C. Abell and F. Hollfelder, *Anal. Chem.*, 2009, **81**, 302-306 (DOI:10.1021/ac802038c; 10.1021/ac802038c).
22 T. Notomi, H. Okayama, H. Masubuchi, T. Yonekawa, K. Watanabe, N. Amino and T. Hase, *Nucleic Acids Res.*, 2000, **28**, E63.
23 N. Tomita, Y. Mori, H. Kanda and T. Notomi, *Nat. Protoc.*, 2008, **3**, 877-882 (DOI:10.1038/nprot.2008.57; 10.1038/nprot.2008.57).
24 Y. Mori and T. Notomi, *J. Infect. Chemother.*, 2009, **15**, 62-69 (DOI:10.1007/s10156-009-0669-9 [doi]).
25 M. Parida, S. Sannarangaiah, P. K. Dash, P. V. Rao and K. Morita, *Rev. Med. Virol.*, 2008, **18**, 407-421 (DOI:10.1002/rmv.593 [doi]).
26 M. Li, F. Diehl, D. Dressman, B. Vogelstein and K. W. Kinzler, *Nat. Methods*, 2006, **3**, 95-97 (DOI:nmeth850 [pii]).

